9th European Workshop on Structural Health Monitoring
July 10-13, 2018, Manchester, United Kingdom

Automated extraction of local defect resonance for efficient non-destructive testing of composites

Joost Segers[1#], Erik Verboven[1], Saeid Hedayatrasa[1,2], Gaétan Poelman[1], Javier Calderon[1], Wim Van Paepegem[1] and Mathias Kersemans[1]

[1] Department of Materials, Textiles and Chemical Engineering (MaTCh), Ghent University, Technologiepark-Zwijnaarde 903, 9052 Zwijnaarde, Belgium

[#] Corresponding author, Joost.Segers@ugent.be

[2] SIM Program M3 DETECT-IV, Technologiepark-Zwijnaarde 935, B-9052 Zwijnaarde, Belgium

Abstract

Local defect resonance (LDR) makes use of high frequency vibrations to get a localized resonant activation of the defect. One of the major difficulties with respect to the use of LDR for non-destructive testing is the actual identification of the LDR frequency. In this study, different post-processing methods are applied to broadband vibration data, obtained for a carbon fiber reinforced plastic with a flat bottom hole, in view of automated extraction of LDR features. LDR detection based on the frequency-domain data analysis is discussed. In order to reduce the computational effort for large datasets, principle component analysis (PCA) and frequency band data (FBD) calculation are investigated. The effect on the calculation time and the data size is investigated. Moreover, a signal-to-noise ratio is introduced to investigate the performance of both techniques with respect to the automated LDR detection algorithm. Finally, the effect of a reduced sampling with respect to the performance of the automated LDR extraction procedure is investigated.

1. Introduction

Composite materials (e.g. carbon fiber reinforced polymer (CFRP) and glass fiber reinforced polymer (GFRP)) are widely used in many advanced engineering structures. Their high specific strength and resistance to fatigue and corrosion makes them especially attractive for transportation applications. A concern in the use of composite materials is related to the occurrence of and sensitivity to internal damage features. The damages are often invisible to the naked eye e.g. barely visible impact damage (BVID). Of utmost importance is a non-destructive testing (NDT) technique that can be used to detect and evaluate small damages.

In 1993, Tenek et al. [1] proposed NDT of composite plates by high frequency modal testing. This technique was further investigated by Solodov et al. [2, 3] during the past decade. The high frequencies are used to get a localized resonant activation of the defected zones and is therefore named: Local Defect Resonance (LDR). The LDR concept is used successfully to detect flat bottom holes (FBH) [4-6], inserts [1, 7, 8], debonding [3, 5] and BVID [4, 7, 9, 10].

In general, the defect's location is revealed by measuring the out-of-plane vibrational surface response of a defected sample using a scanning laser Doppler vibrometer (SLDV).

A major obstacle to the use of LDR as an effective NDT technique is the identification of the LDR frequency (f_{LDR}). An analytical or numerical estimation of the LDR frequencies is possible but only for idealized defects (e.g. flat bottom hole) and on the condition that both the material parameters (e.g. stiffness, density) and the defect characteristics (e.g. size, depth) are known. Obviously the main motivation behind NDT concerns the detection of defects when no a priori information is available. Hence, in reality the LDR frequency cannot be estimated in advance and has to be derived from actual broadband vibrational surface data. This is generally done by manual peak-picking in the frequency response function (FRF) and by analyzing the corresponding operational deflection shapes (ODS).

In the present study, different post-processing techniques are applied to raw scanning laser Doppler vibrometer (SLDV) measurement data in order to automate the detection of LDR and to improve the defect assessment. Their performance is evaluated for measurement data obtained for a CFRP plate containing a flat bottom hole (FBH). First, the experimental procedure is outlined. Next, the different data processing functions are explained and their performance (in frequency domain) is discussed. Finally, the most important conclusions are summarized.

2. Experiment and problem statement

This study focusses on the post-processing of measurement data for a CFRP plate with a circular FBH (see Figure 1). This is a popular type of artificial defect which shows a clear LDR behavior [5]. The sample measures 150 x 90 x 5.52 mm^3 and is manufactured from unidirectional carbon fiber according to layup $[(45/0/-45/90)]_{3s}$. The FBH has a diameter of 10 mm and a remaining material thickness of 2.06 mm.

The sample is suspended using an elastic band at each corner and is excited using a low power piezoelectric (PZT) patch (type EPZ-20MS64W from Ekulit, with a diameter of 15 mm), glued to the back surface (see Figure 1). A burst chirp signal (i.e. fast swept sine with a duty cycle of 90%) from 5 to 100 kHz is used as excitation signal. This signal is amplified 50 times by a Falco System WMA-300 amplifier resulting in a peak-to-peak voltage of V_{pp} = 100 V. The in-plane and out-of-plane vibrational response is obtained by using a 3D infrared scanning laser Doppler vibrometer (Polytec PSV-500-3D XTRA). The infrared wavelength shows excellent sensitivity, even for black CFRP surfaces. Orthogonal projection is used to calculate the velocity of vibration in the X, Y and Z directions, where Z is defined as the out-of-plane component. The front side of the sample is scanned and the orange box marked on Figure 1 indicates the scanned area. Table 1 summarizes the measurement settings. The scan point spacing depends on the desired defect tolerance limit. In this case, the spacing is set to 1.5 mm in order to be able to detect defects > 36 mm^2.

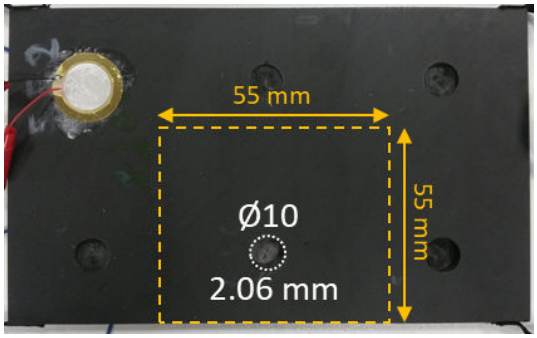

Figure 1: CFRP test specimen with FBH.

Table 1: LDV measurement settings.

	Value
# Scan points	1402
Scan time (s)	93
Scan point spacing (mm)	1.5
Sampling frequency (kHz)	250
# samples per point	10 000
V_{pp} (V)	100
f_{min} (Hz)	1
f_{max} (Hz)	100 000

Figure 2 shows the FRF of a measurement point inside the defected area and the average FRF of the global sample. This figure indicates the difficulty to distinguish between global mode shapes and LDR behavior by analyzing the average FRF (and even the nodal FRF in the defected zone). By careful manual inspection of the ODS at multiple FRF peaks, a clear LDR behavior of the FBH is discovered at 66.4 kHz. As this approach is labor intensive, time consuming and operator dependent, it prevents the further use of LDR as an effective NDT technique. To solve this problem, this study focusses on an automated LDR extraction algorithm. Figure 3 shows the corresponding flow chart of which the three main components (i.e. automated LDR detection, time domain and frequency domain) are explained individually in the next sections.

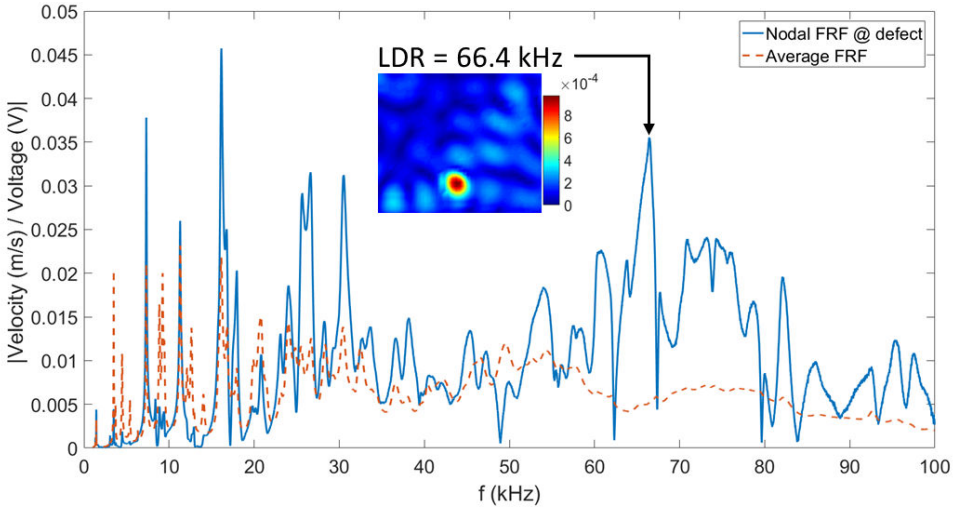

Figure 2: Average (red) and nodal (blue) frequency response function for a $[0/90]_{6s}$ CFRP with a FBH

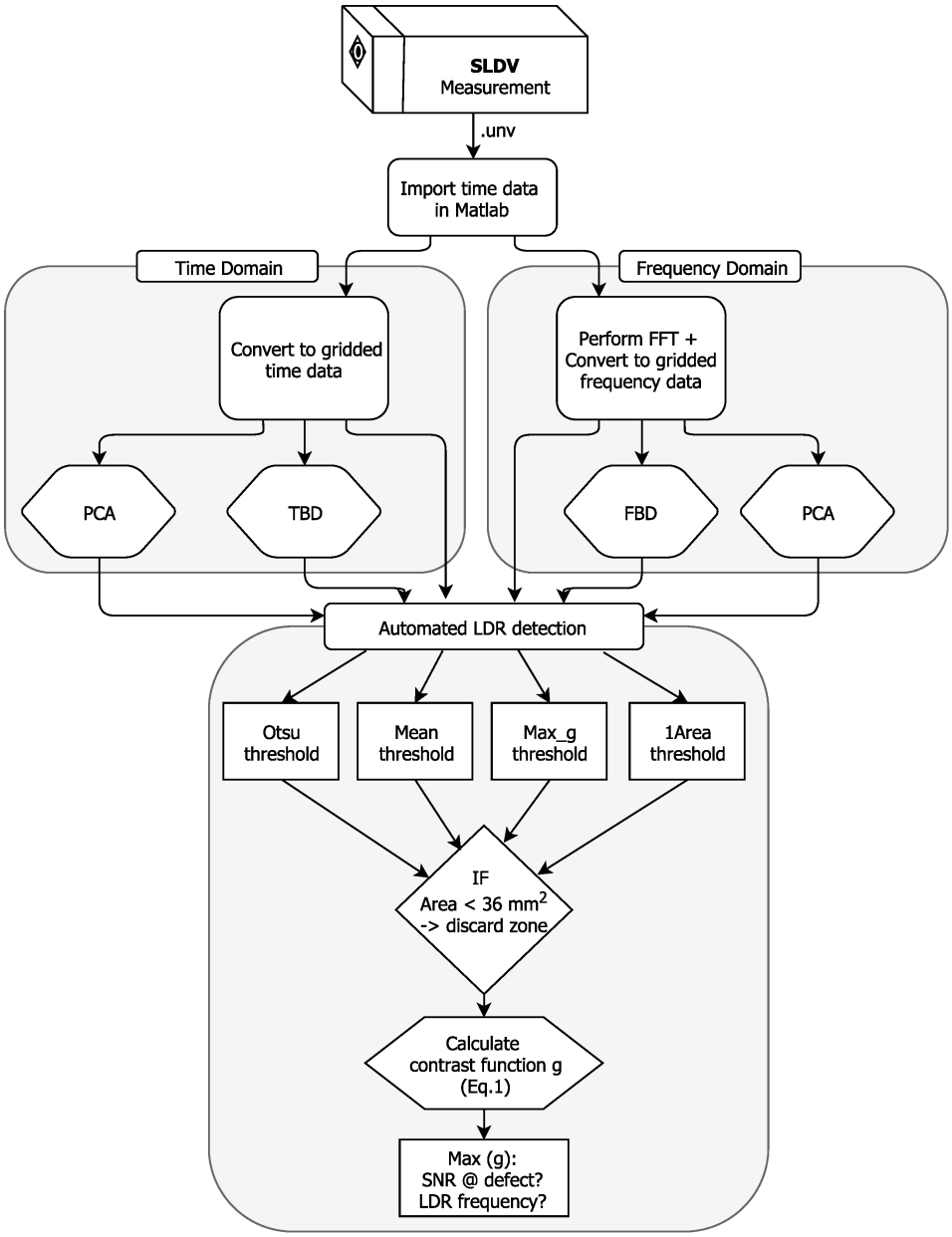

Figure 3: Data processing flow chart.

3. Automated LDR detection

LDR behavior is characterized by a high vibrational amplitude which is very localized. As such, in order to automatically detect this behavior, a contrast function (g) is defined which reaches a maximum when an ODS under investigation shows the LDR characteristics. The contrast function is calculated as:

$$g = \begin{cases} \dfrac{n - n_{thres}}{n_{thres}} \cdot \dfrac{\sum_{(x_i,y_i)\in\Omega_{thres}} V_z(x_i, y_i)}{\sum_{(x_i,y_i)\notin\Omega_{thres}} V_z(x_i, y_i)} \cdot \dfrac{\text{Area}_{(x_i,y_i)\notin\Omega_{thres}}}{\text{Area}_{(x_i,y_i)\in\Omega_{thres}}} & if\ \Omega_{thres} \neq \emptyset \\ 0 & if\ \Omega_{thres} = \emptyset \end{cases} \quad (1)$$

where n is the total amount of data points, n_{thres} is the amount of data points inside the thresholded area Ω_{thres} and $V_z(x_i,y_i)$ represents the out-of-plane velocity amplitude at the data point with coordinates (x_i,y_i). Before g can be calculated, the Ω_{thres} needs to be determined.

This is done by thresholding the ODS under investigation in order to obtain a binary image, in which the white area Ω_{thres} shows a high vibrational intensity compared to the black area. Four different thresholding methods are evaluated, namely: *Otsu's* method, *mean* thresholding, *1area* thresholding and *max_g* thresholding. *Otsu* thresholding is a statistical operation performed on the histogram of the image which maximizes the between-class variance [11]. For *mean* thresholding, the threshold value is chosen identical to the mean pixel intensity of the image. The *max_g* thresholding corresponds to the threshold at which the contrast function *g* reaches a maximum value. In case of *1area* thresholding, the threshold value is increased starting from the *Otsu* threshold until only one contiguous area $\Omega_{thres}>36\ mm^2$ remains. This value corresponds to the defect tolerance limit in certain aerospace applications.

Because LDV measurement errors typically also result in a very localized (typically 1 pixel) increase in the value for the velocity amplitude, care has to be taken not to identify these measurement errors as LDR behavior. Note that these measurement errors can be easily removed by taking into account averages, though on the expense of a higher experimental time. In this study, it is assumed that typical defects are 36 mm^2 in size or larger. As a result, area's smaller as 36 mm^2 showing increased vibrational amplitude are ignored and removed from the total threshold region Ω_{thres}.

The contrast function calculation procedure outlined above is graphically shown in Figure 3. When applied to a large dataset of vibration intensity images (e.g. ODS), this procedure allows to automatically detect the image which shows LDR behavior as this image will correspond to the maximum *g* value. There are multiple sources for the dataset of vibration intensity images which can be used as input for this algorithm. First, the datasets available in the frequency domain are discussed together with the results of the contrast function calculation procedure. Next, the datasets available in the time domain are addressed.

4. Frequency domain

The time domain data of the out-of-plane velocity at each measurement point (SLDV measurement) is exported to Matlab. Once imported, the nodal frequency spectra are obtained by performing fast Fourier transformation (FFT). Considering the Nyquist sampling theorem and the frequency of the excitation signal (see Table 1), the FFT dataset used for post-processing is limited to the frequency band from 5 to 100 kHz. This dataset is uniformly mapped over the global scanned area using a linear interpolation scheme. The distance between the grid points is chosen similar to the average distance between the scan points indicated in Table 1.

The automated LDR detection algorithm is applied to the large dataset of 3800 FFT images. The performance of all four thresholding methods is evaluated. Figure 4 shows the resulting four contrast function curves with indications of the maxima. The corresponding ODS are shown in Figure 5 together with their binarized images used in the calculation of Eq.1. The

ODS at the manually determined f_{LDR} = 66.4 kHz and an ultrasonic C-scan with 5 MHz center frequency transducers are also included as references. As can be seen on the figures, the algorithm succeeded in identifying the correct f_{LDR} in case of *Otsu*, *max_g* and *1area* thresholding. For brevity, only the results for *max_g* thresholding are discussed in the remainder of this paper.

The computational effort of the automated LDR detection is quite high due to the large number of FFT images to be processed (see Section 6). In order to reduce this effort, two different data compression functions can be applied, namely: principle component analysis (PCA) and frequency band data (FBD) calculation.

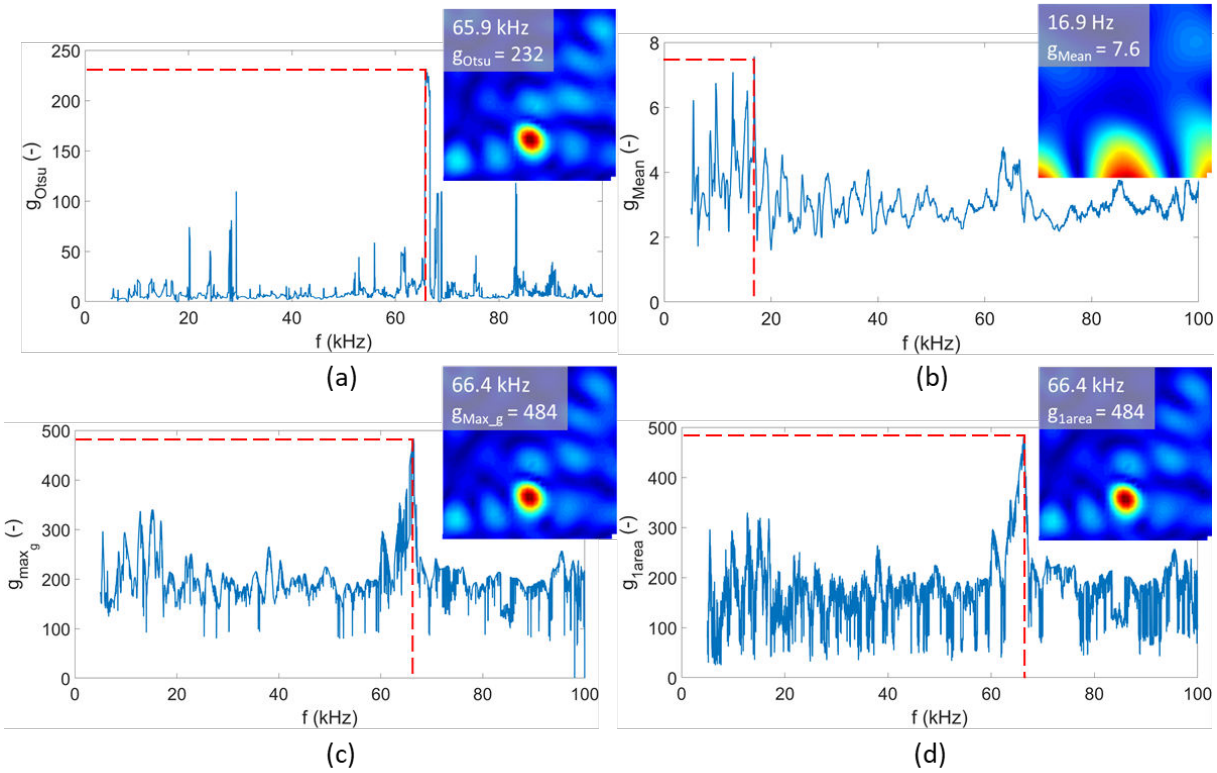

Figure 4: Contrast functions g calculated for all FFT images using (a) Otsu, (b) Mean, (c) Max_g and (d) 1area thresholding.

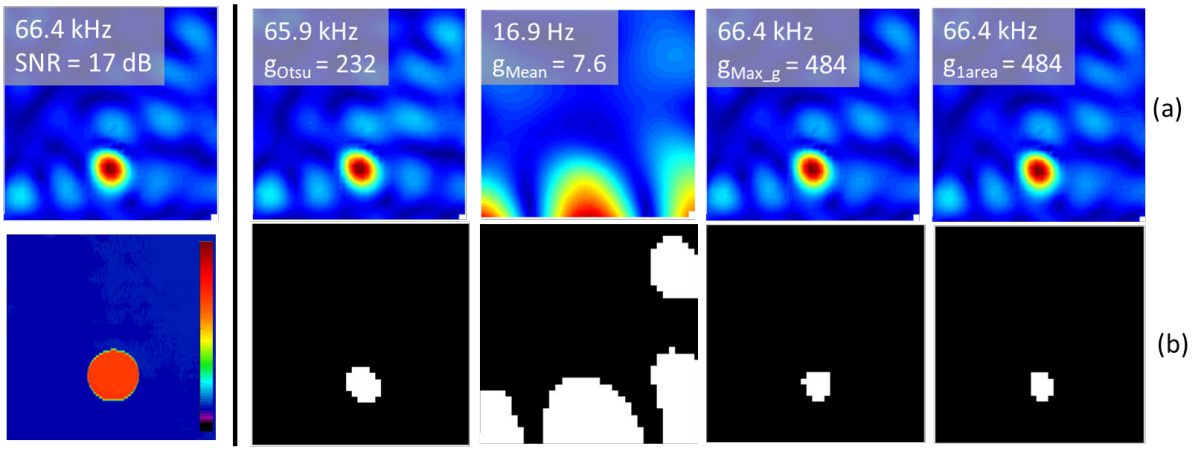

Figure 5: (a) Operational deflection shapes and (b) corresponding binarized images resulting from automated LDR detection applied to all FFT images using Otsu, Mean, Max_g and 1Area thresholding together with the ODS at f_{LDR} and C-scan as a reference.

4.1. Principle Component Analysis (PCA)

PCA is a multivariate technique which aims to extract the important information from a large data table containing observations and to represent it as a limited set of new orthonormal variables called principal components [12]. This analysis approach is popular in thermographic NDT as it allows to compress a large dataset in a few important orthonormal principle components (PC) [13]. Here PCA is used to compress the 3800 FFT images in 100 principle components. The automated LDR detection algorithm is than applied to these 100 images using *max_g* thresholding.

Because for this sample, the damaged area is known, a signal to noise ratio SNR function can be introduced in order to objectively evaluate the performance of PCA (and later FBD). The SNR is defined as:

$$SNR = 20\log\left[\frac{\frac{1}{n_{defect}}\sum_{(x_i,y_i)\in\Omega_{defect}} V_z(x_i,y_i) \quad - \quad \frac{1}{n_{healthy}}\sum_{(x_i,y_i)\notin\Omega_{defect}} V_z(x_i,y_i)}{\sigma_{(x,y)\notin\Omega_{defect}}}\right](dB) \qquad (2)$$

where n_{defect} and $n_{healthy}$ are the number of data points in- and outside the known damaged area (Ω_{defect}) respectively and $\sigma_{(x,y)\notin\Omega_{defect}}$ stands for the standard deviation of the points outside Ω_{defect}. The reduction in SNR due to the data compression technique should be limited as a decrease in SNR reduces the chance of a successful LDR extraction.

Figure 6 (a) shows the first 4 principle components with corresponding SNR. Together, these 4 images explain 48% of variability in the total dataset. Applying the automated LDR detection algorithm to the first 100 PCA images is not successful. Figure 6 (b) shows the 4 PCA images corresponding to the four highest values of the contrast curve g_{Max_g}. Here, the ODS at LDR serves as a reference. The figure indicates that, for this dataset, PCA results in a too large reduction in SNR and as a result, the defect could no longer be identified

automatically. For other types of defects however, the PCA was successful in extracting LDR features in a stable and robust way (not shown due to page limit).

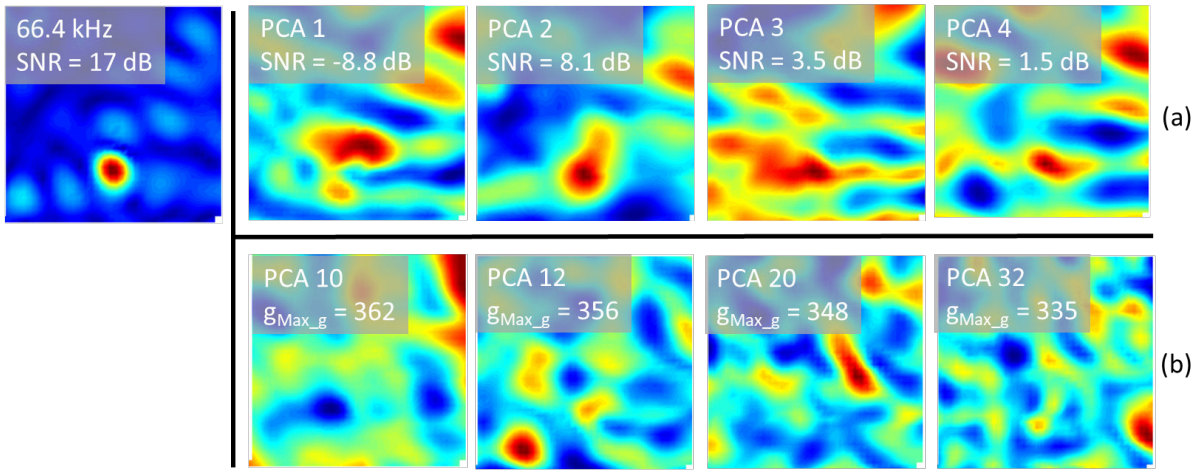

Figure 6: (a) First four PCA images and (b) the four PCA images corresponding to the four highest values of the contrast curve when calculated for all 100 PCA images.

4.2. Frequency Band Data (FBD)

Similar to PCA, FBD calculation is a technique used to compress the large amount of FFT images into a smaller dataset. The FBD of a node at location (x_i,y_i) is defined as:

$$FBD(x_i, y_i, f_1, f_2) = \frac{f_{resolution}}{f_2 - f_1} \sum_{f=f_1}^{f_2} \frac{V_z(x_i, y_i, f)}{U_{Excitation}(f)} \qquad (3)$$

where $f_{resolution}$ is the frequency resolution of the FFT data (i.e. 25 Hz) and f_1, f_2 must lie within the frequency band under investigation (i.e. up to 100 kHz). $V_z(x_i, y_i, f)$ and $U_{Excitation}(f)$ represent respectively the out-of-plane velocity amplitude and the voltage amplitude of the excitation signal supplied to the piezoelectric actuator at the specified frequency *f*. Thus the FBD gives the vibrational amplitude averaged over a frequency band.

As an example, Figure 7 (a) shows the four FBD images for a FBD bandwidth of 25 kHz together with the ODS at f_{LDR} as a reference. Because the vibrational amplitude at LDR is relatively high, the defect is clearly recognizable in the FBD image containing the LDR frequency i.e. 50 to 75 kHz. The presence of the defect is also visible in the adjacent FBD images. This is caused by the increasing vibrational amplitude of the damaged area due to the local reduction in bending stiffness. Note that for this specific bandwidth (i.e. 25 kHz), the original dataset is compressed to only four images. Figure 7 (b) shows the images for which g_{maxg} reaches a maximum when the automated LDR detection algorithm is performed on all FBD images of a bandwidth equal to 10, 20, 50 and 100 kHz respectively. In all cases, the algorithm succeeded in detecting the image containing f_{LDR} and localizing the defect. As indicated on the figure, the SNR of the damaged area is reduced for increasing data compression by FBD but was still sufficiently high to automatically detect the correct image.

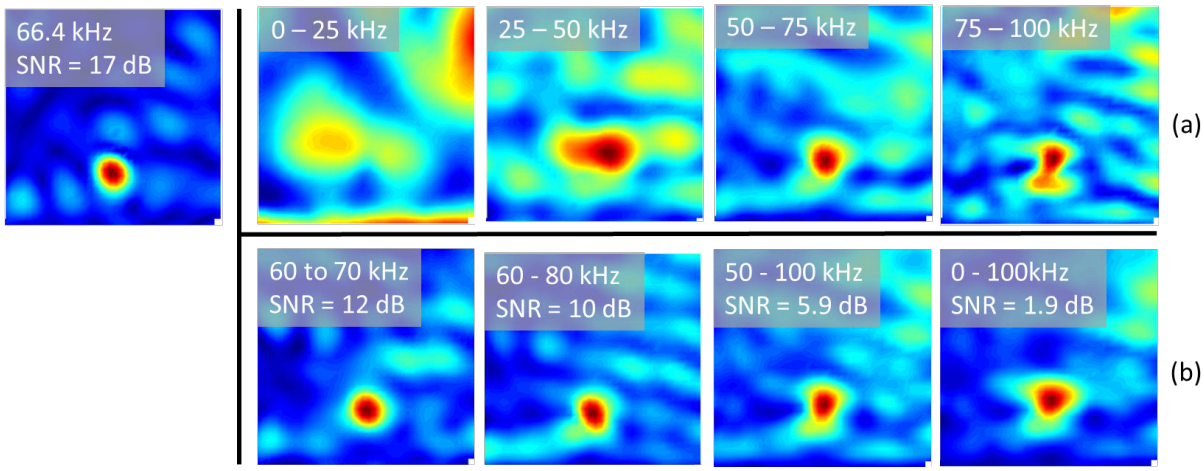

Figure 7: (a) FBD images for a bandwidth of 25 kHz. (b) Automated detected FBD images using g_{Max_g} applied to FBD images calculated for a bandwidth equal to 10, 20, 50 and 100 kHz respectively.

5. Time domain

Instead of performing the data processing in frequency domain, the original nodal time measurement can also be used as input for the automated LDR extraction procedure. The results are highly similar to the results obtained in frequency domain with the difference of the addition of the phase information. This phase information is not used in the frequency domain where the FFT images of the velocity amplitude are used. Similar to the post-processing in frequency domain, the large dataset (now 10 000 images) can be compressed by performing PCA or by averaging the vibrational amplitude over a time band. This last method, is the of counterpart of FBD and is therefore named: time band data (TBD). For brevity however, the results obtained in the time domain are not discussed.

6. Computational effort and number of samples

While the automated LDR detection algorithm proves successful when applied to all FFT images, it is computationally intensive. This is presented in Table 2 which summarizes the calculation times and resulting data sizes for the applied methods. Both the calculation of PCA and FBD decrease the number of input images for the contrast function considerably and thereby reduce the calculation time. The downside is that there is respectively no immediate and a less accurate f_{LDR} prediction. Besides, the SNR after PCA and FBD is lower compared to the SNR at f_{LDR}. This obviously results in a reduced performance of the automated defect detection.

An alternative way to speed up the measurement and calculation time concerns the reduction of the measurement samples. As an example, the SLDV measurement is repeated with 1000 time samples for each point instead of the original 10 000 time samples, which results in a poorer frequency resolution ($f_{resolution}$) of 250 Hz (instead of the original 25 Hz). The advantage is a significant reduction in overall calculation time (see Table 2). The drawback is that the LDR behavior is less distinct (i.e. decreased SNR) and that the f_{LDR} prediction is less accurate. These statements are graphically shown in Figure 8, which shows the SNR and

automated f_{LDR} prediction for a decreasing number of samples (expressed in terms of frequency resolution).

Table 2: Summary of calculation times and resulting data sizes.
(Matlab R2016b without parallelization on PC with 16 GB RAM and an Intel i7 2.90 GHz CPU)

Processing step	Calculation time (s)		Data size (MB)	
	10000 samples (Δf = 25 Hz)	1000 samples (Δf = 250 Hz)	10000 samples (Δf = 25 Hz)	1000 samples (Δf = 250 Hz)
Import .unv file	18.00	6.51	467.70	62.45
Convert to gridded time data	105.90	9.75	224.32	22.50
PCA on time data	9.58	1.86	2.24	1.12
FFT	10.80	1.52	179.46	17.92
Convert to gridded frequency data	38.70	3.84	175.23	18.00
PCA on FFT data	6.06	0.41	1.12	1.12
FBD 10 kHz	0.34	< 0.1	0.11	0.11
FBD 20 kHz	0.27	< 0.1	0.06	0.06
FFT + g_{Otsu}	13.55	1.52	\	\
FFT + g_{Mean}	11.22	1.28	\	\
FFT + g_{max_g}	120.92	15.14	\	\
FFT + g_{1area}	88.61	9.88	\	\

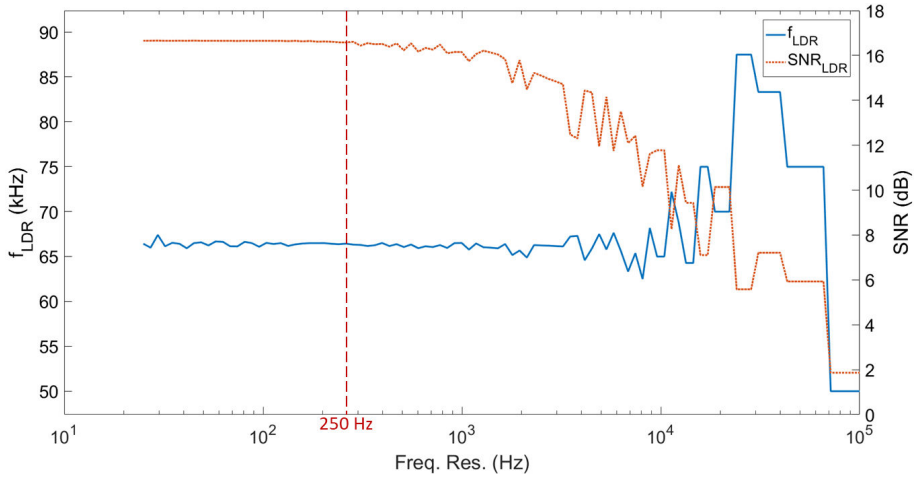

Figure 8: Automated f_{LDR} prediction and corresponding SNR for increasing data compression.

7. Conclusions and future steps

This study addresses one of the major obstacles encountered when using the concept of LDR for NDT, i.e. the automation of the f_{LDR} detection and defect localization. Our procedure has been demonstrated on the broadband vibrational response (recorded using SLDV) of a CFRP plate containing a FBH.

In order to automatically extract LDR behavior in the large dataset of vibration images, an algorithm is proposed which is based on the calculation of a contrast function. This algorithm is applied on data in the frequency domain (but can be equally applied to time domain data). The approach shows a good performance when applied to the large collection of FFT images of the broadband measurement. However, because this procedure is computationally

intensive, two data compression methods are investigated i.e. PCA and FBD. Both methods succeeded in reducing the calculation times considerably but (for the currently considered dataset) the automated LDR detection did not succeed in case of PCA.

With respect to the computational effort, it is also shown that care has to be taken when selecting the number of measurement samples. A high number of samples results in long measurements and calculation times, whereas a too low number of samples decreases the accuracy of the f_{LDR} estimation and, more important, makes the (automated) LDR extraction more difficult.

Further research has to be done towards the performance of the data processing functions for different types of damages e.g. delaminations and impact damage.

Acknowledgments

Joost Segers is a PhD fellow of the Research Foundation-Flanders (FWO, Grant no. 1148018N) and further acknowledges the SBO project DETECT-IV (Grant no. 160455), which fits in the SIM research program MacroModelMat (M3) funded by SIM (Strategic Initiative Materials in Flanders) and VLAIO (Flemish government agency Flanders Innovation & Entrepreneurship).

References

1. Tenek, L.H., E.G. Henneke, and M.D. Gunzburger, *Vibration of delaminated composite plates and some applications to non-destructive testing.* Composite Structures, 1993. **23**: p. 253-262.
2. Solodov, I., *Local defect resonance (LDR): A route to highly efficient thermosonic and nonlinear ultrasonic NDT.* AIP Conference Proceedings, 2014. **1581**(1): p. 1663-1670.
3. Solodov, I., J. Bai, S. Bekgulyan, and G. Busse, *A local defect resonance to enhance acoustic wave-defect interaction in ultrasonic nondestructive evaluation.* Applied Physics Letters, 2011. **99**(21).
4. Solodov, I., *Resonant Acoustic Nonlinearity of Defects for Highly-Efficient Nonlinear NDE.* Journal of Nondestructive Evaluation, 2014. **33**(2): p. 252-262.
5. Hettler, J., M. Tabatabaeipour, S. Delrue, and K.V.D. Abeele, *Detection and Characterization of Local Defect Resonances Arising from Delaminations and Flat Bottom Holes.* Journal of Nondestructive Evaluation, 2017. **36**(1).
6. Sarens, B., B. Verstraeten, C. Glorieux, G. Kalogiannakis, and D. Van Hemelrijck, *Investigation of Contact Acoustic Nonlinearity in Delaminations by Shearographic Imaging, Laser Doppler Vibrometric Scanning and Finite Difference Modeling.* IEEE Transactions on Ultrasonics, 2010. **57**(6): p. 1383-1395.
7. Rahammer, M. and M. Kreutzbruck, *Fourier-transform vibrothermography with frequency sweep excitation utilizing local defect resonances.* NDT and E International, 2017. **86**: p. 83-88.
8. Solodov, I., M. Rahammer, and N. Gulnizkij, *Highly-Sensitive and Frequency-Selective Imaging of Defects via Local Defect Resonance*, in *11th European Conference on Non-Destructive Testing*. 2014: Prague.

9. Fierro, G.P.M., D. Ginzburg, F. Ciampa, and M. Meo, *Imaging of Barely Visible Impact Damage on a Complex Composite Stiffened Panel Using a Nonlinear Ultrasound Stimulated Thermography Approach.* Journal of Nondestructive Evaluation, 2017. **36**(4).
10. Pieczonka, L., L. Zietek, A. Klepka, W.J. Staszewski, F. Aymerich, and T. Uhl, *Damage imaging in composites using nonlinear vibro-acoustic wave modulations.* Structural Control and Health Monitoring, 2017.
11. Otsu, N., *A Threshold Selection Method from Gray-Level Histograms.* IEEE Transactions on Systems, Man, and Cybernetics, 1979. **9**(1): p. 62-66.
12. Abdi, H. and L.J. Williams, *Principal component analysis.* Wiley Interdisciplinary Reviews: Computational Statistics, 2010. **2**(4): p. 433-459.
13. Zhang, H., N.P. Avdelidis, A. Osman, C. Ibarra-Castanedo, S. Sfarra, H. Fernandes, T.E. Matikas, and X.P.V. Maldague, *Enhanced Infrared Image Processing for Impacted Carbon/Glass Fiber-Reinforced Composite Evaluation.* Sensors (Basel), 2017. **18**(1).